THE JOURNAL OF PHYSICAL CHEMISTRY C

Article

pubs.acs.org/JPCC

Mechanisms of Peptide Oxidation by Hydroxyl Radicals: Insight at the Molecular Scale

C. C. W. Verlackt,*[,†] W. Van Boxem,[†] D. Dewaele,[‡] F. Lemière,[‡] F. Sobott,[‡,§,∥] J. Benedikt,[⊥] E. C. Neyts,[†] and A. Bogaerts*[,†]

[†]Research group PLASMANT, Department of Chemistry, University of Antwerp, Universiteitsplein 1, 2610 Antwerp, Belgium

[‡]Biomolecular & Analytical Mass Spectrometry group, Department of Chemistry, University of Antwerp, Groenenborgerlaan 171, 2020 Antwerp, Belgium

[§]Astbury Centre for Structural Molecular Biology, University of Leeds, Leeds, United Kingdom

[∥]School of Molecular and Cellular Biology, University of Leeds, Leeds, United Kingdom

[⊥]Research Department Plasmas with Complex Interactions, Ruhr-Universität Bochum, 44780 Bochum, Germany

Supporting Information

ABSTRACT: Molecular dynamics (MD) simulations were performed to provide atomic scale insight in the initial interaction between hydroxyl radicals (OH) and peptide systems in solution. These OH radicals are representative reactive oxygen species produced by cold atmospheric plasmas. The use of plasma for biomedical applications is gaining increasing interest, but the fundamental mechanisms behind the plasma modifications still remain largely elusive. This study helps to gain more insight in the underlying mechanisms of plasma medicine but is also more generally applicable to peptide oxidation, of interest for other applications. Combining both reactive and nonreactive MD simulations, we are able to elucidate the reactivity of the amino acids inside the peptide systems and their effect on their structure up to 1 μs. Additionally, experiments were performed, treating the simulated peptides with a plasma jet. The computational results presented here correlate well with the obtained experimental data and highlight the importance of the chemical environment for the reactivity of the individual amino acids, so that specific amino acids are attacked in higher numbers than expected. Furthermore, the long time scale simulations suggest that a single oxidation has an effect on the 3D conformation due to an increase in hydrophilicity and intra- and intermolecular interactions.

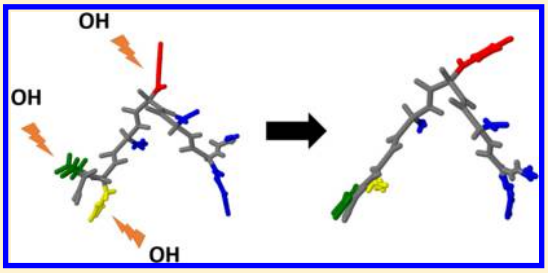

INTRODUCTION

The use of cold atmospheric pressure plasmas (CAPPs) for medical applications, i.e., plasma medicine, has been receiving growing interest in the scientific and medical communities, linking biochemistry, physics, and medicine together.[1,2] The capability to generate a vast range of biochemically important reactive species, reactive oxygen and nitrogen species (RONS), at low temperature, by utilizing an inexpensive, simple, and vacuum-free setup, makes CAPPs a strong tool to be used in various medical fields.[3,4] The success of plasma medicine has been demonstrated in recent years, not only by in vitro studies, but also in multiple in vivo studies for cancer treatment,[5−7] wound and ulcer healing,[4,8−10] and dental treatment.[11]

The main role of CAPPs in this field is the generation and transport of RONS to the cells of interest. Among these species are singlet oxygen ($O_2\ ^1\Delta_g$), superoxide anions (O_2^-), hydroxyl radicals (OH), oxygen atoms (O), hydrogen peroxide molecules (H_2O_2), nitric oxide (NO), and peroxynitrite ($ONOO^-$). Most of these species are known to take part in several cellular pathways and signaling. Although they often have a short lifetime and the plasma acts on the surface of the treated tissues, the biological responses to the treatment are observed over longer distances and depths, over larger time scales, and even inside the affected cells.[12−18] These longer time scale events and biological responses build up as a result of the initial interactions between the plasma generated species and the treated area of the tissue. Knowledge on the initial interactions, as well as the resulting effects, is thus crucial in order to better understand the biological responses toward plasma treatment.

In order to gain knowledge of the processes that occur, insight in the direct interactions between the generated reactive species and the biochemical structures, at the molecular scale, is crucial. To date, a large amount of research has already been performed to better understand these interactions and the subsequent oxidation in the case of lipids, DNA, and amino acids.[19−26] However, knowledge involving the interactions of RONS with peptides and proteins remains limited. To better understand the plasma−protein interactions, we perform here molecular dynamics (MD) simulations, combining both

Received: December 6, 2016
Revised: February 21, 2017
Published: February 22, 2017

DOI: 10.1021/acs.jpcc.6b12278
J. Phys. Chem. C 2017, 121, 5787−5799

reactive MD using the density-functional based tight-binding (DFTB) method and nonreactive MD calculations, to provide molecular-scale understanding of the expected oxidation processes for two small peptides, i.e., angiotensin fragment 1−7 and bradykinin, serving as simple model systems for proteins. We specifically look at the interactions between the peptides and OH radicals, being representative for the RONS created by the plasma.[27] We focus on OH radicals, because previous studies have indicated that OH radicals are most reactive toward the biomolecular structures,[27] able to react within the limited time scales (i.e., picosecond ranges for DFTB). The interactions are investigated in the presence of water and molecular oxygen, as proteins and peptides during treatment are usually found in aerobic water. Furthermore, the presence of O_2 might play an important role in the propagation of radical oxidation of biomolecules.[28,29] To validate the computational investigation, we also perform experiments, treating the model peptides with a microscale atmospheric pressure plasma jet, after which the oxidation and possible structural changes are investigated.

COMPUTATIONAL SETUP

Figure 1 illustrates the chemical structure of both peptides investigated. In this representation the amide bond in the backbone is depicted in red and it is shortened for the sake of clarity (see figure A for more details). The investigated peptides are modeled after angiotensin fragment 1−7 (a hormone responsible for vasoconstriction, called peptide A in this work) and bradykinin (an inflammatory mediator, called peptide B in this work), respectively. Both peptides have the advantage of being relatively small−with a size best suited for the calculations−and containing enough variation in the structure (i.e., type of amino acids) without being too complex. Furthermore, these peptides are relatively easy to purchase, for experimental validation of the computations, and they have already been the subject of various studies in literature.[30,31] Sulfur containing amino acids (i.e., cysteine and methionine), which are known to be easily oxidized, are not present in the current study. Recognizing the importance of covalent modifications of such amino acids during plasma treatment, they will, however, be subject for further investigation in the near future.

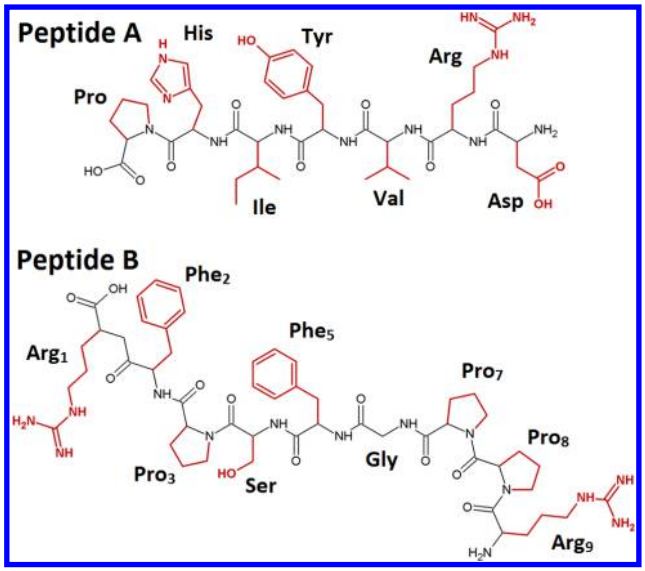

Figure 1. Chemical structure of the peptides considered for the reactive MD simulations: Angiotensin fragment 1−7 (called here peptide A) and bradykinin (peptide B). In this representation the amino acid side groups are depicted in red.

The chemical reactions between OH radicals and both model peptides were investigated using reactive MD simulations (which will be referred to as impact simulations) utilizing the DFTB method. DFTB is a computational technique which utilizes a Taylor series expansion of the Kohn−Sham total energy as used in DFT calculations.[32] In this investigation, so-called third order DFTB (i.e., DFTB3 complemented with the 3ob-2-1 parameter set) was used, which employs the third series expansion of the mentioned energy equation resulting in a self-consistent computational method. As a result, DFTB3 is able to accurately describe highly charged biomolecules, hydrogen binding energies, proton affinities and proton transfers, for systems up to 10^3 atoms, as it takes into account the charge dependence of the chemical hardness of individual atoms.[33,34] More information can be found in the work of Gaus et al.[34]

Our preliminary simulations pointed out that the oxidation reactions are initiated by OH radicals, followed by an interaction with molecular oxygen. This observation inspired us to perform our computational study in three steps:

(I) A total of 75 impact simulations, each containing 2 OH radicals, were performed using the DFTB method for each peptide (A and B) in the presence of water molecules, in order to elucidate the expected oxidation sites.

(II) Based on this information about the most targeted reaction sites, further oxidation processes were investigated using the respective amino acids in the presence of molecular oxygen. The results were validated using experimental data from literature, to be sure that we obtained the most common and expected oxidation products for each amino acid.

(III) Subsequently, the most common oxidation products were implemented in the peptides to investigate their effect on the structural behavior using a nonreactive force field (GROMACS).

This approach is necessary, given the nature of the employed reactive MD simulations, i.e., DFTB, which is a quite time-consuming calculation method. Indeed, we chose to investigate the further oxidation processes in step II on isolated amino acids rather than on every oxidized peptide observed in step I, in order to limit the necessary calculation expenses and to guarantee the occurrence of later-stage oxidation reactions at the sites of interest. In fact, if these calculations would be performed on the oxidized peptides of step I, only a very small fraction of the introduced species would react with the amino acids of interest (i.e., which were targeted in the previous step).

In the first step, we treated isolated peptides in each impact simulation. Given the size of the peptides, positioning the structure inside a water box or inside a water-shell would surpass the size limitation of the used method, i.e., 10^3 atoms, as stated before. However, to account for the effect of surrounding water molecules on the interactions, and thus to better mimic reality, we introduced the OH radicals in an aqueous sphere (see Figure 2). In this way, the radicals are surrounded by water molecules at the moment of impact, without the need to have water molecules surrounding the complete peptide. However, it

DOI: 10.1021/acs.jpcc.6b12278
J. Phys. Chem. C 2017, 121, 5787−5799

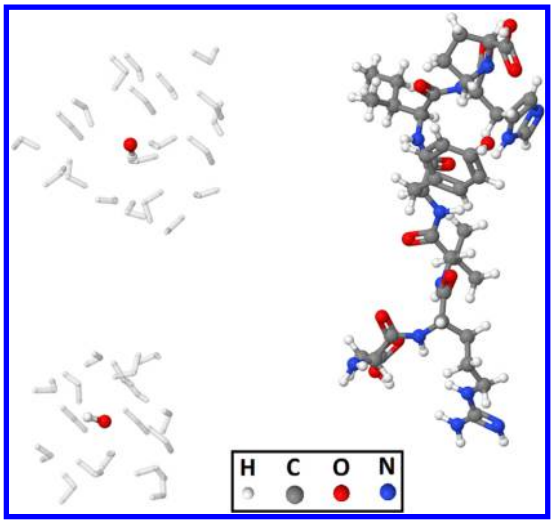

Figure 2. Snapshot of the initial 3D structure of peptide A as used in the impact simulations. Two OH radicals are placed inside a water shell, to ensure no initial interactions with the peptide and to mimic the effect of the surrounding water molecules on the interaction process during the impacts.

should be noted that due to the lack of an aqueous solution, no charges are implemented in the investigated peptide, as it is treated in vacuum.

In the second step, we considered isolated amino acids, and the OH radicals (or O_2 molecules) were not surrounded by water this time. This might affect the reactivity to some extent. Indeed, OH radicals will have a lower chemical hardness in solution, resulting in an overall lower reactivity toward biomolecules.[35] This behavior has been observed during our peptide impact simulations and also in our earlier studies.[23] However, the purpose of this step was to obtain information on every possible oxidation product, rather than to obtain statistically valid distribution of products. The obtained oxidation products were compared to experimental data from literature, to reveal which are the most common and expected oxidation products to be used in the third step of this investigation (see below).

For both the peptide and amino acid impact simulations, a simulation time of 10 ps was chosen, to ensure that chemical reactions occur within the time scale of the simulation while maintaining reasonable calculation times. The impact simulations were performed in a canonical ensemble (temperature and volume were kept constant, NVT) using a Berendsen thermostat with a coupling constant of 100 fs. All simulations were performed using periodic boundary conditions for a cubic box with dimensions of 25 × 25 × 25 Å for the amino acids, and 40 × 40 × 40 Å for the peptides. Prior to the impact simulations, all systems were equilibrated at room temperature for 100 ps using similar simulation conditions. All impact simulations were performed using a time step for integration of 0.25 fs.

Finally, the obtained oxidation products of the second step, i.e., the impact simulations on the most targeted amino acids, were introduced to the respective peptide and used to perform nonreactive MD simulations in water, to obtain insight into the effects of the oxidation products on the structural behavior of each peptide. The nonreactive MD simulations were performed using the GROMACS 5.1.2 package.[36,37] Six different structures were prepared for each peptide: the native structure, three structures containing a single oxidized amino acid, one structure containing two oxidized amino acids, and one containing three oxidized amino acids (as determined from the reactive MD simulations; see details in the Section Nonreactive MD Simulations below). All structures were dissolved in a 40 × 40 × 40 Å box containing TIP3P water molecules, and periodic boundary conditions were applied on all three dimensions. Due to the small dimensions, the effects of pH could not be considered in this investigation. Indeed, as the simulation box can only contain around 2100 water molecules, the introduction of even a single proton will lead to an acidic solution (with a pH of 4.5 or lower). The native and oxidized structures were equilibrated at 300 K and 1 atm using the Nose-Hoover thermostat and Parrinello−Rahman barostat. The particle mesh Ewald (PME) method was used to treat the long-range electrostatic interactions. A total simulation time of 1 μs was used with a time step of 1 fs. A principle component analysis (PCA), also known as essential dynamics, was used for analyzing the structural modifications. During a PCA, a covariance matrix is built, which embodies the collinearity of atomic motions for each pair of atoms. This matrix, in turn, is diagonalized, and the sum of the eigenvalues is a measure for the total mobility of the analyzed system, while the eigenvectors describe the collective motion of the particles.

EXPERIMENTAL DETAILS

A microscale atmospheric pressure plasma jet (μ-APPJ) operated in He/O_2 gas mixture is used to treat liquid samples (Figure 3). It is a capacitively coupled microplasma jet

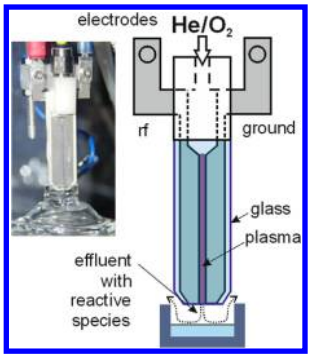

Figure 3. Photograph and a scheme of the μ-APPJ used in the treatment of the test solutions.

consisting of two stainless-steel electrodes (length 30 mm, width 1 mm) with 1 mm electrode distance, where the electrode gap is confined on both sides by quartz glass plates. A discharge is generated in the volume of 1 × 1 × 30 mm^3 by applying a radio frequency (rf) voltage (13.56 MHz, root-mean-square voltage 230 V, absorbed power P_{plasma} < 1 W) to one electrode, where the other one is grounded (see Figure 3). This electrode configuration and corresponding dimensions resemble very closely the recently introduced plasma-jet reference discharge, the COST-Jet.[38]

The plasma is operated with 1.4 standard liter per minute helium flow with 8.4 standard cubic centimeter of O_2 gas per minute (0.6% of He flow). Maximum O atoms density (8 × 10^{14} cm^{-3}) in the effluent is obtained at these conditions at 4 mm distance at the position of the liquid surface.[39] The O atoms enter effectively aqueous solutions and can oxidize any dissolved organic molecules. We have argued recently that O

DOI: 10.1021/acs.jpcc.6b12278
J. Phys. Chem. C 2017, 121, 5787−5799

atoms directly, rather than OH radicals generated in $H_2O + O \rightarrow 2OH$ reaction, are reacting in the liquid; however, the resulting products of O and OH reactions are similar.[40] Given the similarity in the reactions induced by both OH and O, we decided to only introduce OH radicals in our simulations in order to better control the observed reactions and limit the computational expenses. Indeed, the O atoms are expected to mainly react by means of H-abstraction reactions,[41] forming an OH radical, an immediate consecutive reaction is expected.

Angiotensin fragment 1−7 and bradykinin were obtained from Sigma-Aldrich (Bornem, Belgium). Reverse osmosis (RO) water was prepared using a Silex water filtering system from Eurowater (Nazareth-Ekeren, Belgium). 7.5 M ammonium acetate solution was purchased from Sigma-Aldrich (Bornem, Belgium). Acetonitrile (ACN; HPLC grade for analysis) and formic acid (FA; 99+%) were obtained from Acros Organics (Geel, Belgium). Samples were diluted to a concentration of 1 mg/mL and 400 μL aliquots were placed in glass vials. The final concentration of the plasma-treated samples was determined after exposure, since the gas jet resulted in some solvent evaporation.

The effect of the plasma treatment was studied using an ESI-Q-TOF Synapt G2 HDMS T-wave ion mobility mass spectrometer (Waters, Wilmslow/UK). Samples were diluted to 5 μM and introduced into the instrument by nano-electrospray ionization (ESI) in positive ion mode, using gold-coated borosilicate capillaries made in-house (capillary voltage 1.25−1.5 kV). Adduct formation was monitored under denaturing conditions (50:50:1 H_2O:ACN:FA) and in TOF mode, while ion mobility (IM) measurements were done using native-like solution conditions (100 mM aqueous ammonium acetate pH 6.9) in IM mode. The sample and extraction cone voltage were set in the range of 20−40 V and 0.5−1.0 V, and source and desolvation temperatures were 50° and 150°, respectively. Vacuum pressures were backing 2.46 mbar, source 1.79×10^{-3} mbar, trap 6.2×10^{-2} mbar, and transfer cell 6.3×10^{-3} mbar. For the IM experiments the following parameters were used: He and IM cell gas flow 180 and 90 mL/min; DC bias 45 V, wave height 40 V, and wave velocity 700 m/s. The mass range was set to 50−2000 Da. External calibration up to 2000 m/z was performed with NaI/CsI solution. Data acquisition was performed using MassLynx (version 4.1).

RESULTS AND DISCUSSION

Peptide Impact Simulations. The first step in this investigation was performed to gain insight in the most favored sites for initiating the oxidation in both peptides upon OH radical impact. This was done by performing 75 independent impact simulations for each peptide, as described in the Computational Setup. After 10 ps, 41, and 49% of the OH radicals have reacted with peptide A and B, respectively. The results of the impact simulations are summarized in Table 1 and Figure 4.

During the simulations, the OH radicals mainly reacted through H-abstraction reactions. The H atoms in the peptides that are mostly prone to abstraction by the OH radicals are presented by the red spheres in Figure 4. The intensity of the red color is a measure for the number of H-abstraction reactions that were observed on that particular site. Hence, it is clear that the OH radicals mainly target the hydroxyl group of serine (Ser) in peptide B and of aspartic acid (Asp) and tyrosine (Tyr) in peptide A (see intense red spheres on the mentioned amino acids in Figure 4). In addition, also the first

Table 1. Summary of the Observed Oxidations and the Amino Acids That Were Targeted by the OH Radicals Introduced During the Peptide Impact Simulations[a]

	percentage of oxidation (%) compared to the total number of reactions observed		
amino acid oxidized	peptide A	peptide B	
Arg	9	Arg_1	4
		Arg_9	22
Asp	**34**		np
Gly	np		**3**
His	**18**		np
Ile	**2**		np
Phe	np	**Phe_2**	**10**
		Phe_5	**0**
Pro	18	Pro_3	14
		Pro_7	4
		Pro_8	12
Ser	np		**19**
Tyr	**20**		np
Val	**0**		np

[a]The percentages correspond to the number of oxidation reactions that occur at the respective amino acid, compared to the total number of reactions observed (not including reactions on both terminals of the peptide). np: not present in peptide. Bold: only present in the corresponding peptide.

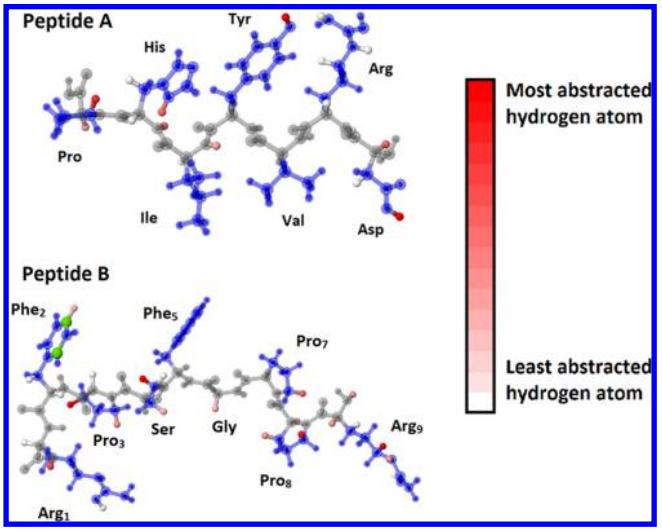

Figure 4. Snapshot of the 3D representation of the oxidation sites in both peptides. The H atoms most prone to H-abstraction reactions are depicted as red solid spheres, using a scale ranging from pale to intense red, representing the range from least abstracted to most abstracted H atoms. The green spheres indicate the positions where OH addition reactions were observed. Atoms which did not react with OH radicals are depicted in transparent blue (for the side groups) or gray (for the peptide backbone).

arginine (Arg_9) of peptide B, and the proline (Pro) in both peptides, are attacked in high numbers by the introduced OH radicals. Finally, H-abstraction reactions have also been observed on Arg_1 in peptide B and on both the aromatic amino acids, i.e., histidine (His) in peptide A and phenylalanine (Phe_2) in peptide B, albeit to a lesser extent (indicated by the light red spheres on the mentioned amino acids). The percentage of oxidation is summarized in Table 1.

Besides H-abstraction, also some OH addition reactions are observed, but only for peptide B (i.e., 3% of the reactions), and

DOI: 10.1021/acs.jpcc.6b12278
J. Phys. Chem. C 2017, 121, 5787−5799

the C atoms that are subject to these OH addition reactions are indicated by green spheres in Figure 4. This reaction was, however, only observed on Phe_2 of peptide B. The side groups and peptide backbone where no OH reactions took place are depicted in transparent blue and gray, respectively. These results indicate that the OH radicals favor (i) the hydroxyl and carboxyl groups found in both peptides as well as (ii) the side groups of the amino acids in both peptides. Looking at Table 1, it is clear that in the case of peptide A, reactions were mainly observed to happen on Asp, followed by Tyr, Pro, and His, and finally Arg and isoleucine (Ile) (see Table 1). The order of oxidation for Tyr, His, Arg, and Ile is in agreement with experimental observations.[21,29,42] Takai et al. investigated the oxidation of every individual amino acid as a result of plasma jet treatment.[21] They reported that chemical modifications were mostly encountered on amino acids containing a sulfur atom or aromatic group, such as Tyr and His, while the concentration of oxidized Arg and Ile was significantly lower compared to Tyr and His, in agreement with our simulations. Furthermore, Stadtman reported that Tyr, His, and Arg are indeed among the amino acids that are susceptible for oxidation by ROS,[29] while Ile has not been mentioned, supporting the low reactivity observed in our simulations. Moreover, the oxidation of Tyr and His has also been encountered in a recent study by Lackmann et al.[42]

On the other hand, in our simulations, Pro and Asp are affected by the OH radicals more often than initially expected. In the case of Asp, this is a result of the presence of the carboxyl group, one of the main targets of the impacting species. This functional group is expected to be deprotonated in aqueous solution at pH ∼7 (pK_a value of 3.86). Given the low number of water molecules present during the simulations, we decided to investigate the neutral equivalent of the peptide, instead of the deprotonated variant, similar to the terminal carboxyl group. Furthermore, the high hydrophilicity of the carboxyl group makes it easier for the OH radicals, residing inside an aqueous shell, to come in contact with Asp, significantly increasing the chance of oxidation. In the case of Pro, we observe that peptide A folds into a specific 3D structure during the simulation. This structure leads to a relatively large potential contact surface for the targeted Pro with the solution, which possibly explains the higher-than-expected number of observed reactions, surpassing the number of reactions on His (see structure in Figure 5).

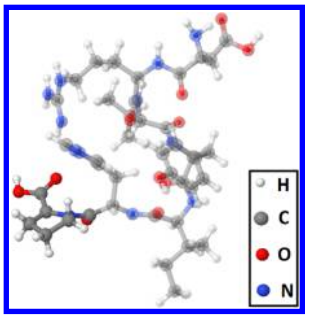

Figure 5. Snapshot of peptide A after 10 ps. Proline is found to have a relatively large contact surface with the solution. This might explain the higher number of observed reactions, compared to experiments. Proline is represented by the solid spheres while the remaining peptide is depicted using semitransparent spheres, for the sake of clarity.

For peptide B, most OH reactions took place on Pro (mostly Pro_3 and Pro_8), Arg (Arg_9 and in rare cases Arg_1), Ser, Phe_2, and finally glycine (Gly). The order of Pro, Arg, and Gly is in line with observations reported in literature.[21,29] Indeed, while Pro and Arg are known to be susceptible to ROS oxidation, the reactions with Gly are rarely encountered experimentally. However, the observed oxidation rate of Phe is significantly lower compared to experimental reports.[21,29] Being an aromatic amino acid, Phe is known to be even more susceptible to oxidation than Pro and Arg and comparable to Tyr.[21] The lower reactivity, observed in our simulations, might be the result of the impact conditions, where aqueous spheres around the OH radicals are introduced, while the peptide itself is not dissolved (in order to avoid excessive calculations times). Before the introduced OH radicals can interact with the peptide, the amino acids must first come in contact with the aqueous shell. Given the apolar nature of Phe, one can expect that the interaction with the water shell is less favored, compared to, for example Arg, Pro, and even Tyr. Moreover, as Phe is able to occupy a larger phase space compared to Pro, i.e., being more flexible, while Pro is more fixed in the peptide structure, the repulsion from the impacting water-radical droplets is expected to be more pronounced in the case of Phe. This can explain the lower number of observed oxidation reactions with Phe. Finally, Ser is targeted to a similar extent as the aromatic Tyr and appears more reactive than expected from literature. However, this can be explained by the high hydrophilicity compared to its environment, similar to Asp for peptide A. This makes it easier for the OH radicals to come in contact with the hydroxyl group of Ser while this is not the case for Tyr, resulting in similar numbers of oxidation (see Table 1).

The differences in the observed reactivity for Phe and Ser (in peptide B), as well as for Asp (in peptide A), illustrate the importance of the chemical environment of the amino acids for oxidation by ROS. This importance has recently been reported by Espino et al.,[43] who observed, among others, a surprisingly high oxidation rate of Asp, which was attributed to the fact that this amino acid is a marker for solvent accessibility.[44] The influence of the chemical environment is especially clear when comparing the difference in reactivity of the same amino acids occurring more than once in the peptide (i.e., Pro, Arg, and Phe in peptide B). Indeed, Table 1 clearly illustrates a significantly higher number of oxidations of Phe_2 compared to Phe_5, of Pro_3 and Pro_8 vs Pro_7, as well as of Arg_9 compared to Arg_2.

The observation that the OH radicals react somewhat more with peptide B than with peptide A (i.e., 49% vs 41%) correlates well with experimental data obtained after plasma treatment of both model peptides. Figure 6 illustrates the obtained mass-spectra of both model peptides after 1 min treatment using the μ-APPJ. The difference in both spectra after plasma treatment is very striking. It is clear that peptide B is indeed more prone to oxidation during the experiments. The reason for this striking difference and the resistance of peptide A toward ROS oxidation remains unclear and will be subject to further investigation. However, this can possibly be attributed to the increase in peptide flexibility after later stage oxidation of proline (as bradykinin contains three proline groups), which in turn enhances further oxidation. Indeed, overoxidation of proline found in peptide B leads to the opening of its ring structure after which the characteristic bends in the backbone disappear,[21,29] giving more "space" for oxidation. As already mentioned, the difference between the rates of oxidation of

DOI: 10.1021/acs.jpcc.6b12278
J. Phys. Chem. C 2017, 121, 5787−5799

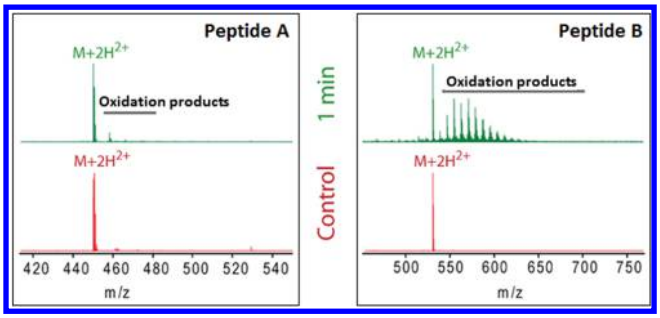

Figure 6. ESI mass spectra of angiotensin fragment 1−7 (peptide A) and bradykinin (peptide B) under denaturing conditions, after 1 min of plasma treatment using a μ-APPJ. Covalent adducts appear at m/z values higher than the peptide mass, with each major peak corresponding to n additional oxygen masses ($n \times 16$ Da). While peptide A shows predominantly only one oxygen adduct ($n = 1$), peptide B gets oxidized up to >10 times under the same conditions.

peptides A and B is only subtly observed during the computational investigation. However, it should be noted that the simulations were performed under vacuum conditions where the effects of solvation, pH, ions, and charges are not included due to the limitations of the used method. Indeed, in our computational study only the effect of water molecules is taken into account when considering the radical interactions. On the other hand, no buffer solutions have been used to control the pH value, which was, therefore, at the standard value for reverse osmosis water in contact with air (~5.5−6, not measured). Moreover, the treated peptides were bought as acetate salts. These conditions can play a role in the oxidation processes. This might explain the observed difference between the rates of oxidation of peptide A and B compared to the simulated results.

Amino Acid Impact Simulations. Based on the knowledge obtained from the peptide impact simulations, the most targeted amino acids, i.e., three for each peptide, were selected for investigating the further oxidation processes of these amino acids. Keeping in mind the comparison with literature (see above), we selected Tyr, His, and Pro for peptide A and Phe_2, Pro_1, and Arg_1 for peptide B (see Scheme 1). More specifically, the further oxidation of Tyr is investigated after the abstraction of the hydroxylic hydrogen atom; for His, further oxidation is studied after the abstraction of the N-bound hydrogen atom; for Arg, after the abstraction of the C_3-bound hydrogen atom; for Phe, after the addition of the OH radical on position C_4 in the ring; and for Pro (occurring in both peptides A and B), after the abstraction of the C_4-bound hydrogen atom. Their further oxidation processes were simulated by introducing either an O_2 molecule or another OH radical to the amino acid in vacuum. Asp was not considered in these further oxidation simulations, given the fact that the oxidation is focused on the carboxyl group by abstracting the H atom, which is absent in aqueous solution at pH ~7, as discussed above. It should be noted that the final products as depicted in Scheme 1 are not end products of oxidation. Indeed, further oxidation of these products will occur during experiments and for longer time scale simulations. The chosen products are a result of interacting with only a single, or two, OH radicals in the presence of molecular oxygen.

For every case, 10 independent impact simulations were performed in a system containing only a single oxygen species (i.e., either an OH-radical or O_2 molecule). A summary of the observed reactions is presented in Scheme 1. Introducing oxygen species to the amino acid radicals results in either H-abstraction adjacent to the atom containing the unpaired electron, leading to the formation of a C═C or C═N double bond, or addition of the OH radical or O_2 molecule on the radical site. The specific reactions observed for each of the amino acid radicals are explained below in more detail, along with the most probable follow-up reactions. The formation of 3,4-dihydroxyphenylalanine and 2-oxohistide (see Scheme 1) were not simulated as this requires much larger time scales and more complex molecular systems, beyond the limitations of DFTB. However, below we motivate why they should arise from the amino acid radicals observed in our simulations. Hence, these final products are also depicted in Scheme 1, because they will be used in the later nonreactive MD simulations (see below).

The Tyr radical reacts with OH radicals through addition on the C_3 atom, positioned next to the hydroxyl functional group. This results in the formation of Tyr-C_3OH (top left Scheme 1). It is noteworthy that within the time scale of 10 ps, no chemical reaction occurred with O_2, showing the stability of the initial amino acid radical during these calculations. Although reactions on aromatic structures progress slowly during the simulations, the formation of Tyr-C_3OH was observed multiple times. Furthermore, the illustrated addition reaction is a well-known result of tyrosine oxidation and is in excellent agreement with the literature, resulting in the precursor for 3,4-dihydroxyphenylalanine (DOPA).[21,25,29,45−48] DOPA will be formed after a H-abstraction from neighboring biomolecules or H-donors by Tyr-C_3OH. However, this could not be simulated in this work, as the required time scale exceeds the capabilities of DFTB. Indeed, after the H-abstraction of Tyr, no consecutive H-abstraction was observed during the peptide impact simulations, supporting the need for longer simulation times.

The His radical was able to react with both OH radicals and O_2 molecules, resulting in the formation of three distinct products: His-CC, His-C_3O, and His-C_1OH (see Scheme 1 for nomenclature). First, His-CC results from H-abstraction of C_0 adjacent to the ring structure, by OH radicals. His-C_1OH results from OH addition on the tertiary C_1 in the imidazole ring structure, but it was observed less frequently than the formation of His-CC. Finally, O_2 molecules react through addition on the N═C−N carbon atom in the ring (C_3), resulting in the formation of a peroxyl radical (His-C_3O). Peroxyl radicals are known to undergo a number of reactions, resulting in the formation of hydroxyl and carbonyl derivates.[25,45,49]

Among these reaction products is the formation of 2-oxohistidine, a well-known product of histidine oxidation.[21,25,29,48,49] In order to acquire 2-oxohistidine, a number of reduction processes with either Fe^{2+} in the presence of H^+ or reduction through additional H-abstraction reactions from neighboring H-sources are required.[29] Simulating the reduction of His-C_3O therefore requires both significantly longer time scales (similar to the formation of DOPA) and more complex molecular systems (necessary to introduce the H-sources or perform metal-catalyzed reactions), which are beyond the capabilities of the DFTB method used. However, as 2-oxohistidine is observed to be the major oxidation product of His,[25,29,48,49] it is used for the nonreactive simulations for peptide A, as described in the next section.

The Pro radical shows reactions with both OH radicals and O_2 molecules, similar to His. Both oxygen species interact with

DOI: 10.1021/acs.jpcc.6b12278
J. Phys. Chem. C 2017, 121, 5787−5799

Scheme 1. Observed Reactions between the Amino Acid Radicals, Formed in the Peptide Impact Simulations (See Previous Section) and the Introduced Oxygen Species, i.e., Either OH or O_2, as well as the Later Stage Oxidation Products, Either Obtained from the Simulations (Solid Arrow) or Proposed from Experiments in Literature (Dashed Arrows)[a]

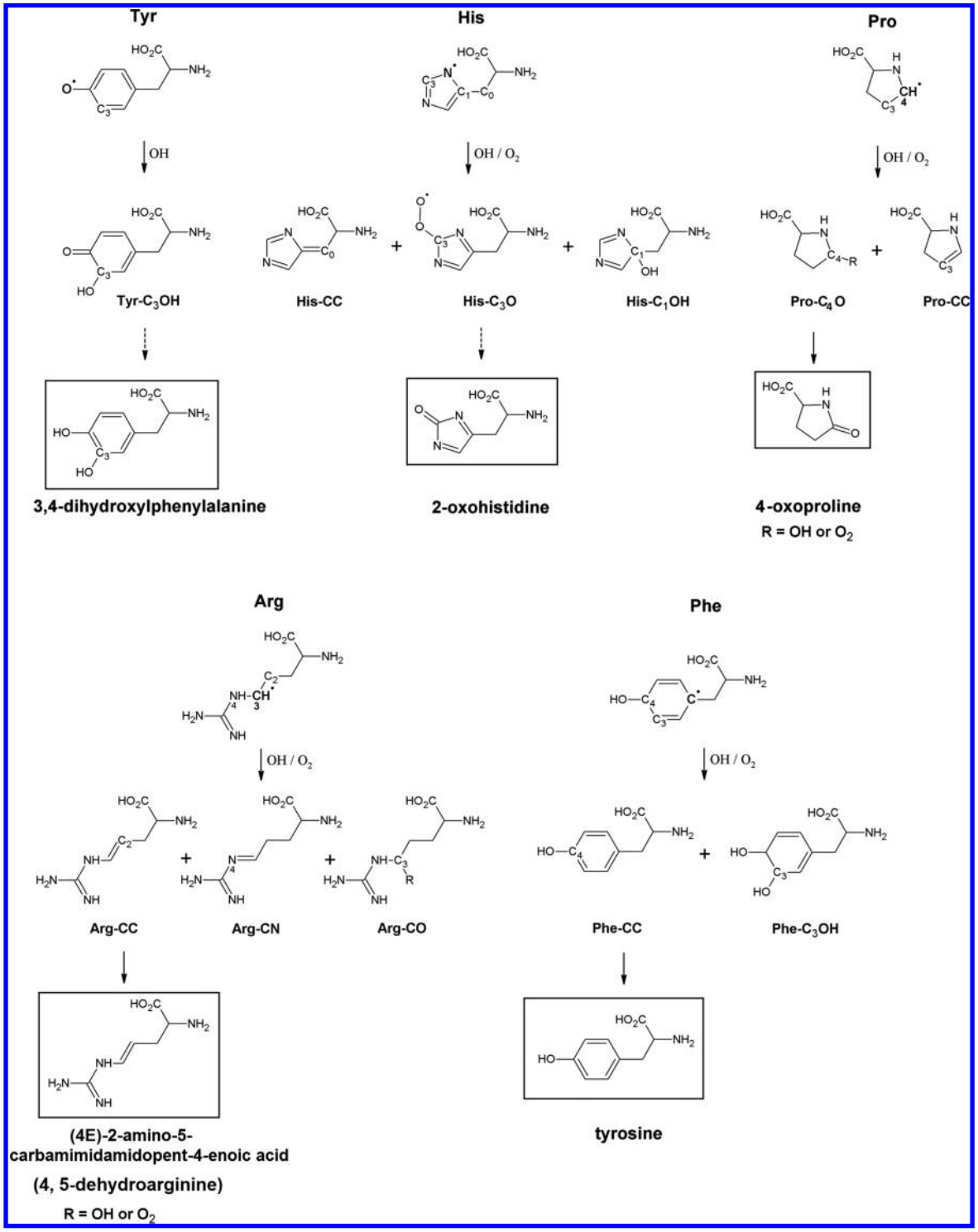

[a]The latter could not be observed in the simulations, as it would require longer time scales and more complex molecular systems, which are far beyond the limitations of DFTB. The reactions displayed for Tyr, His, and Arg are related to peptide A, while those for Phe, Pro, and Arg are connected to peptide B. For each amino acid, a single (later stage) oxidation product was chosen, indicated in rectangular boxes, to be used in the non-reactive MD simulations (see below). Note that O_2 did not react with the Tyr-radical within the simulated time scale.

the radical through either an addition reaction on C_4, resulting in the formation of Pro-C_4O (adding either a peroxide or a hydroxyl group on the pyrrolidine ring), or an H-abstraction reaction on C_4, leading to the formation of Pro-CC (see Scheme 1 for nomenclature). Although the oxidation of Pro was not so often investigated in the literature, it is known to result in an increase in the oxygen content in the pyrrolidine ring structure, forming, among others, 2-pyrrolidone, 4- or 5-

DOI: 10.1021/acs.jpcc.6b12278
J. Phys. Chem. C 2017, 121, 5787−5799

hydroxyproline, and 4-oxoproline.[21,29,50] As 2-pyrrolidone is a product after peptide-bond cleavage and the addition of oxygen species has been encountered on the C_4 of Pro during the simulations (Pro-C_4O in Scheme 1), we have chosen to include 4-oxoproline in the nonreactive MD simulations for both peptides A and B (see next section). Note that the formation of 4-oxoproline was only encountered during our simulations when Pro-C_4O was formed after an OH addition (R = OH in Scheme 1). Similar to 2-oxohistidine, further reactions with the observed Pro-C_4O peroxide, as a result of an O_2 addition (R = O_2 in Scheme 1), were not simulated as the required conditions exceed the capabilities of DFTB.

Introducing oxygen species in the vicinity of the Arg radical results in the formation of multiple oxidation products. During the simulations, both OH radicals and O_2 molecules were able to abstract a H atom from the C_2 and N_4 atoms adjacent to the radical. This leads to the formation of Arg-CC and Arg-CN, respectively (see Scheme 1 for nomenclature). Next to the H-abstraction reactions, addition reactions on C_3 were also encountered during the simulations, leading to the formation of Arg-CO. The oxidation at this particular position is in line with known oxidation products of Arg, e.g. glutamic semialdehydes and the formation of double bonds.[21,29] For the last step of this investigation, Arg-CC, or (4E)-2-amino-5-carbamimidamido-pent-4-enoic acid (will be referred to as 4,5-dehydroarginine for the sake of simplicity), see Scheme 1, was chosen for peptide B, as the formation of this double bond is observed in experimental research[21] using only mild oxidative stress.

Finally, Phe radicals were observed to react with both OH radicals and O_2 molecules to form Phe-CC, after a H-abstraction by either oxygen species, thus restoring the aromatic system, or Phe-C_3OH, upon addition of an OH radical on C_3 (see Scheme 1). The restoration of the aromatic system, after the H-abstraction, results in the formation of tyrosine and has been observed both experimentally as well as during previous computational studies.[19,21,48] Therefore, tyrosine will be introduced in the nonreactive MD simulations for peptide B.

Nonreactive MD Simulations. Based on the peptide impact simulations, and the subsequent individual amino acid impact simulations, six structures were identified for both peptides A and B, to be investigated with the longer time scale nonreactive MD simulations (see Table 2). These structures include the native structures (called A-Nat and B-Nat, respectively), three structures per peptide containing a single oxidation product (A-Tyr, A-His, A-Pro, B-Phe, B-Arg, and B-Pro), one structure per peptide containing two oxidation products (A-ox2 and B-ox2, respectively) and one containing three oxidation products (A-ox3 and B-ox3, respectively). For these modified structures, the indicated amino acids of the native structure were replaced by their respective oxidation products as depicted in Scheme 1. The structures were dissolved in a 40 × 40 × 40 Å water box and simulated for 1 μs.

The results of these nonreactive MD simulations are illustrated in Figure 7. Here the PCA analyses of all structures, plotting the projection of the first eigenvector of the analysis (representing the direction of the highest motion) versus the projection of the second eigenvector (representing the second highest motion) are presented. These graphs give a representation of the total phase space that each peptide is able to occupy. In Table 3, we also list the covariance values, i.e., the sum of the eigenvalues, for each structure, providing a numerical representation of the total motility of the respective

Table 2. Summary of the Peptide Structures Used for the Nonreactive MD Simulations[a]

	peptide A		peptide B	
	AA oxidized[c]	name	AA oxidized[c]	name
native[b]		A-Nat		B-Nat
one oxidation product	Tyr	A-Tyr	Phe_2	B-Phe
	His	A-His	Pro_8	B-Pro
	Pro	A-Pro	Arg_9	B-Arg
two oxidation products	Tyr	A-ox2	Phe_2	B-ox2
	His		Pro_8	
three oxidation products	Tyr	A-ox3	Phe_2	B-ox3
	His		Pro_8	
	Pro		Arg_9	

[a]Six structures were investigated for both peptides A and B: the native structure, three peptides containing a single oxidation product, a peptide containing a combination of two oxidation products and a peptide containing the combination of all three oxidation products. [b]Native structure as depicted in Figure 1 [c]The mentioned amino acids (AA) were replaced by their respective oxidation product, as given in Figure 6.

structures. In the top two graphs of Figure 7, the introduction of a single oxidation product is compared with the native structure for both peptides A and B, while in the bottom two graphs of Figure 7 the effect of introducing an increasing number of oxidation products in shown.

The results in Figure 7 indicate that even a single oxidation product can affect the overall structural behavior of the peptide in which it is introduced, albeit to a low extent. This is apparent for A-Tyr compared to A-Nat. For peptide A a significant reduction of the phase space is observed when Tyr is replaced with 3,4-dihydroxylphenylalanine, i.e., the oxidation product of Tyr. This is also obvious when comparing the covariance value of both structures (9.53 nm^2 versus 16.22 nm^2). This observation points toward a more rigid structure after the oxidation of Tyr, which can affect the overall behavior of the hosting protein. Indeed, as the local structure of the protein (in the vicinity of the oxidized Tyr) changes due to oxidation, so will the interactions with other proteins or receptors on and inside cells. As such, the observed oxidation product can enhance or hinder the protein activity due to the key-lock principle, which greatly depends on the protein considered.

However, for the other oxidation products, the effect on the peptide structure is much less pronounced. Although the projections of the eigenvectors suggest some slight changes in the phase space, the covariance values are considered equal to each other. We were not able to perform a statistical analysis of the covariance values due to the major computational cost required for such calculations. However, in order to obtain a measure for the fluctuation of the covariance values, simulations of 4 structures (A-Nat, A-Tyr, A-ox2, and A-ox3) were repeated a second time. This allows us to verify both the changes in phase space of A-Tyr, as well as the limited effect of further oxidation (A-ox2 and A-ox3). Covariance values similar to those reported in Table 3 were calculated (see SI-1 for the values) and an overall fluctuation of ±2 nm^2 was observed. Therefore, this number is used here as a measure for the fluctuation, when comparing the covariance values of the investigated structures. Based on this number, the calculated covariance values of the oxidized structures (with exception of A-Tyr) are considered to be equal compared to their native counterparts. This indicates that slight changes in the overall

DOI: 10.1021/acs.jpcc.6b12278
J. Phys. Chem. C 2017, 121, 5787−5799

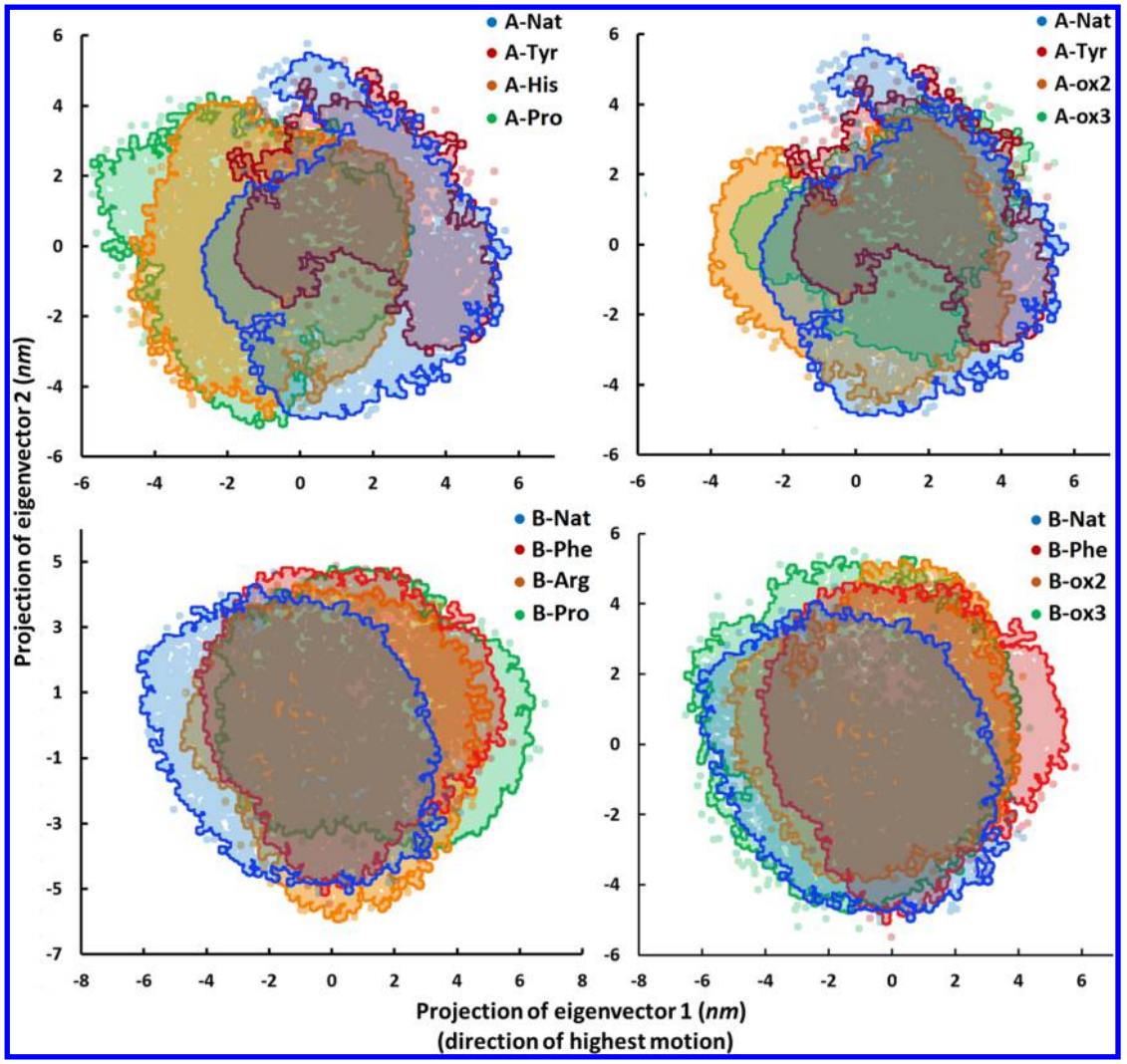

Figure 7. Results of the principle component analysis (PCA) performed on each structure after 1 μs. In the left two graphs the PCA results are shown for the native structures (A-Nat and B-Nat, respectively) compared to the structures containing one of the three oxidation products, as summarized in Table 2. In the right two graphs the PCA results are shown for the native structures compared to the structures containing an increasing number of oxidized amino acids (comparing the phase space that is occupied by peptides with 0, 1, 2, or 3 oxidation products).

Table 3. Summary of the Covariance Values (in nm^2) after 1 μs for the Native Structures and Each of the Modified Structures of Both Peptides A and B

peptide A		peptide B	
structure	covariance value (nm^2)	structure	covariance value (nm^2)
A-Nat	16.22	B-Nat	22.68
A-Tyr	9.53	B-Phe	27.12
A-His	18.18	B-Arg	25.97
A-Pro	18.68	B-Pro	25.71
A-ox2	20.06	B-ox2	24.30
A-ox3	16.05	B-ox3	26.89

structure are expected, without a change in the flexibility as well as the average size of the peptide.

The absence of significant changes in the flexibility and average size is supported by experimental data, obtained with "native" ion mobility mass spectrometry (IM-MS) for the two peptides after 1 min of plasma treatment, as presented in Figure 8.[51,52] In order to obtain experimental insight into the global structural effects of peptide oxidation, four extracted IM-MS profiles are shown and compared: the native structure in the control (i.e., untreated) sample (M + 2H^{2+}, red); the native (unoxidized) structure in a treated sample (M + 2H^{2+}, green); the structure containing one additional oxygen atom (M+O +

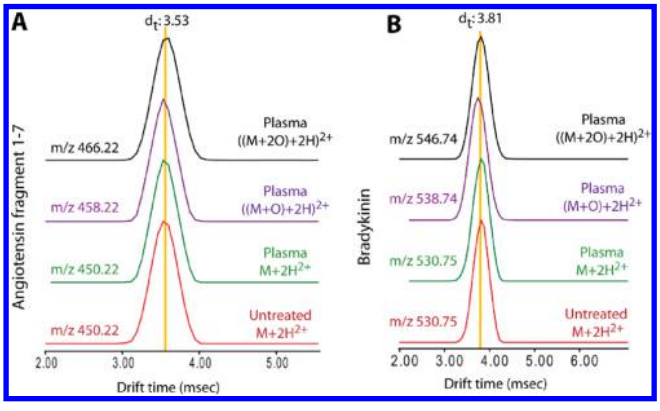

Figure 8. Extracted ion mobility profiles of (A) angiotensin fragment 1−7 and (B) bradykinin after 1 min of plasma treatment. No significant differences are found for the overall size and shape of the peptides with and without up to two oxygen adducts.

DOI: 10.1021/acs.jpcc.6b12278
J. Phys. Chem. C 2017, 121, 5787−5799

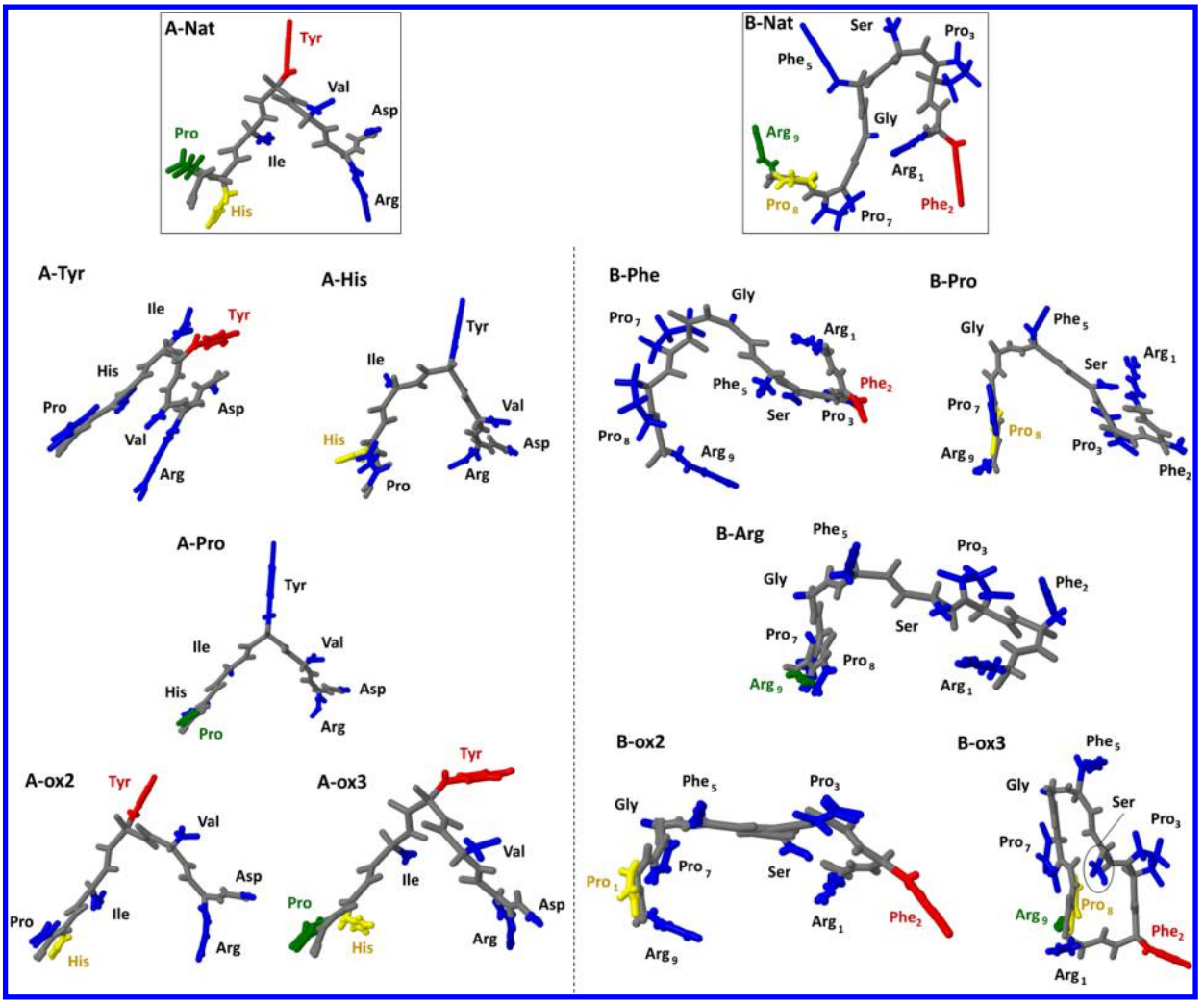

Figure 9. Representation of the average structures of the native peptides (black boxes) and their oxidized structures. On the left side the structures of peptide A are shown, on the right side the structures of peptide B. The peptide backbone is depicted in gray using a stick model in all structures. Unoxidized side groups are depicted in blue. Red indicates the oxidation of Tyr for peptide A and Phe for peptide B. Yellow indicates the oxidation of His for peptide A and Pro for peptide B. Green indicates the oxidation of Pro for peptide A and Arg for peptide B.

$2H^{2+}$, purple); and the structure containing two additional oxygen atoms ($M+2O + 2H^{2+}$, black). Comparing the signals, we observe no significant change in drift time when the peptides (both peptide A and B) are oxidized after plasma treatment. The drift time in IM-MS characterizes ions based on their rotationally averaged size and shape (collision cross section), as well as intrinsic flexibility (conformational space, via the width of the mobility peaks). Therefore, the results suggest that oxidation has no noticeable effect on the overall 3D structure or folding state of the peptide, which is in agreement with the results of the PCA of Figure 7 and Table 3.

As the results of both the PCA and IM-MS experiments show no major structural differences between the oxidized peptides and the native peptides, we also compared the average structures of the peptides after 1 μs in solution, in order to obtain additional insight in the 3D structures. These structures are depicted in Figure 9. In these figures the average position of every atom, compared to the center of mass, is depicted. Note that this does not represent a physical molecule, but rather a visualization of the most likely positions of each atom in this molecule (for example: as the phenyl ring of Phe is only able to rotate around its axis, the average structure will illustrate all atoms to be on that axis). In these figures the backbone is shown in gray, while the unmodified side groups are depicted in either blue. The red, yellow and green side groups represent the amino acids that were considered for oxidation, as specified in Table 2.

From the native peptides A and B, a certain 3D configuration is obtained from calculations (see Figure 9, black boxes). Peptide A appears to exhibit a more linear configuration with a distinctive bend around Val-Tyr-Ile. This conformation has also been found using NMR and circular dichroism by Lula et al.[30] On the other hand, peptide B shows a more random conformation, with interactions between the H and O atoms of different amides in the backbone, found throughout the simulation (see SI-2).

Oxidation of some amino acids in the peptides has an impact on the structural properties and therefore also on the conformation of the peptides. This could not be clearly deduced from the PCA or the IM-MS spectra, but it is obvious from the average positions of all atoms in the oxidized peptides, which are also illustrated in Figure 9. When comparing the modified structures with their native counterparts, it becomes clear that even a single oxidized amino acid can significantly

DOI: 10.1021/acs.jpcc.6b12278
J. Phys. Chem. C 2017, 121, 5787−5799

affect the average conformation. In most cases, this results in a more compact environment where the oxidized amino acid shows a stronger interaction with the peptide backbone, reducing the local surface area. For example, the introduction of 4-oxoproline or 2-oxohistidine results in a slightly higher affinity of the introduced oxidized amino acids for the backbone and neighboring side groups, leading to a more condensed conformation at the site of oxidation itself (see A-His, A-Pro and B-Pro, compared to the native structures). However, the general effect is, again, most pronounced for the oxidation of Tyr in peptide A (see A-Tyr). The increase in affinity with the backbone of Tyr in this modified peptide A results in an additional bend in the peptide, resulting in a more folded structure. This observation is, however, much more subtle in the case of A-ox2 and A-ox3. Indeed, although the oxidized amino acids are found more closely to the peptide (His, Pro, as well as Tyr), the folding of the conformation (as seen in A-Tyr) is prevented in the case of these higher oxidation degrees. The reliability of the obtained structures has been tested by simulating the initial structures of A-Nat, A-Tyr, A-ox2, and A-ox3 a second time for 1 μs (results are shown in the SI-3), and very similar average conformations were obtained; hence, identical observations could be made, supporting the results and the discussion made above.

A similar conclusion can be drawn for peptide B, where the oxidation of Pro and Arg results in a more compact conformation at the respective sites, similar to A-Pro and A-His. However, compared to peptide A, a higher degree of oxidation has a much more pronounced effect on the structure (see B-ox2 and B-ox3). The reason for the more pronounced differences of B-ox2 and B-ox3, however, remains unclear and might be a result of a more random 3D structure, as this effect has not been observed during the PCA. Indeed, if the peptide is more flexible during the MD simulations, this will have a larger effect on the average structure. In this case, we expect that the introduction of more than 1 oxidation product reduces the stability of the conformation of peptide B, increasing both the amount of interactions with the solution and the fluctuation of the 3D structure. As a result, the obtained average structures differ more from the native peptide.

It has been indicated in the literature that oxidation of proteins results in significant protein deformation, leading to either protein accumulation (i.e., the formation of aggregates of several proteins) or the loss of the 3D structure.[53] From the average structures presented above we observe an increase in affinity between the oxidized amino acids and the peptide. This increase in affinity can, besides causing changes in protein activities, also be linked with the experimentally observed aggregation of proteins, as a result of more and stronger intermolecular interactions. Protein aggregation tends to be insoluble as well as resistant to metabolic activities and is associated with cell death in many diseases (Alzheimer's and amyloid diseases, Parkinson's disease, etc.).[54] In contrast, accumulation is prevented in unstressed cells as a result of cellular enzymatic activities. As the oxygen content increases, so will the hydrophilicity, which results in a higher contact surface with the solution. Because of this, important disulfide bonds and amino acids are more available for oxidation, leading to a further loss of the structure and activity, and even fragmentation, finally destroying the affected protein.[42,53]

CONCLUSION

In this work we used atomic scale simulations to investigate the interactions between OH radicals and small peptides, as well as the further oxidation processes of selected amino acids in these peptides, and the effect of these oxidation products on the structural behavior of the peptides. Furthermore, the calculations were compared with experimental data obtained by plasma oxidation of peptides. As model peptides, we considered a part of angiotensin (i.e., fragments 1−7) and bradykinin, as they are both small enough to be effectively treated in reactive MD simulations, they contain enough structural variation (i.e., occurrence of various amino acids), and they could easily be purchased for experimental validation.

The computational work was performed in three steps. The first two steps are based on reactive MD simulations, using the DFTB method, in order to study the oxidation of both peptides by OH radicals within a time scale of 10 ps and in the presence of O_2. In most cases this resulted in H-abstraction, but in rare occasions also a direct OH addition reaction was observed. This resulted in a rise in carbonyl and hydroxyl groups on the side groups of the amino acids, leading to an increase in the oxygen-content of the peptide. The amino acids that were mainly targeted within both peptides correspond well with experimental data from literature, and the reasons for the higher reactivity for some amino acids were provided.

In the third step, we implemented a number of the observed oxidation products in both peptides, in order to elucidate the effect of these products on the structural properties of the peptides in aqueous solution over a time scale of 1 μs. The PCA results did not show any clear effects on the phase space occupied by the oxidized peptides, compared to their native counterparts. This was supported by IM-MS data for both peptides. Here, Tyr proved to be an exception, as we encountered a significant decrease in flexibility, but this effect was again reversed when a second oxidation product was introduced in the peptide. Nevertheless, from the average position of the atoms within the structures, we can conclude that the oxidation of even a single amino acid can affect the average 3D conformation, without changing the size of the peptide.

From our results it is clear that the oxidation of amino acids is greatly dependent on their chemical environment, as well as the contact surface with the solution. Furthermore, we observed that even a single oxidation is able to induce changes in the 3D conformation of the peptide. We expect that this will influence the structural properties of the affected protein as a whole, leading to changes in their enzymatic activities, possible accumulation of proteins, as well as the loss of the 3D conformation. Our work provides additional insight in the expected oxidation mechanisms even when mild oxidative stress is inflicted on proteins and biological tissues, as a result of cold atmospheric pressure plasma treatment.

ASSOCIATED CONTENT

Supporting Information

The Supporting Information is available free of charge on the ACS Publications website at DOI: 10.1021/acs.jpcc.6b12278.

Calculated data (i.e., covariance values IS-1 and average structures IS-3) of the second batch of calculations as well as an example of the observed intrapeptide interactions of bradykinin (SI-2). (PDF)

DOI: 10.1021/acs.jpcc.6b12278
J. Phys. Chem. C 2017, 121, 5787−5799

AUTHOR INFORMATION

Corresponding Authors

*E-mail: christof.verlackt@uantwerpen.be. Tel: +32-(0)3-265.23.62. Fax: +32-(0)3-265.23.43.

*E-mail: annemie.bogaerts@uantwerpen.be. Tel: +32-(0)3-265.23.77.

ORCID

C. C. W. Verlackt: 0000-0002-8063-6708

Notes

The authors declare no competing financial interest.

ACKNOWLEDGMENTS

The authors acknowledge financial support from the Fund for Scientific Research—Flanders (Project Number G012413N) and from the Hercules foundation for the Synapt G2 IM-MS instrument. The calculations were performed using the Turing HPC infrastructure at the CalcUA core facility of the Universiteit Antwerpen, a division of the Flemish Supercomputer Center VSC, funded by the Hercules Foundation, the Flemish Government (department EWI) and the Universiteit Antwerpen.

REFERENCES

(1) von Woedtke, T.; Reuter, S.; Masur, K.; Weltmann, K.-D. Plasmas for Medicine. *Phys. Rep.* **2013**, *530*, 291−320.

(2) Isbary, G.; Zimmerman, J. L.; Shimizu, T.; Li, Y.-F.; Morfill, G. E.; Thomas, H. M.; Steffes, B.; Heinlin, J.; Karrer, S.; Stolz, W. Non-Thermal Plasma—More Than Five Years of Clinical Experience. *Clin. Plasma Med.* **2013**, *1*, 19−23.

(3) Kong, M. G.; Kroesen, G.; Morfill, G.; Nosenko, T.; Shimizu, T.; van Dijk, J.; Zimmermann, J. L. Plasma Medicine: an Introductory Review. *New J. Phys.* **2009**, *11*, 115012.

(4) Emmert, S.; Brehmer, F.; Hänßle, H.; Helmke, A.; Mertens, N.; Ahmed, R.; Simon, D.; Wandke, D.; Maus-Friedrichs, W.; Däschlein, G.; et al. Atmospheric Pressure Plasma in Dermatology: Ulcus Treatment and Much More. *Clin. Plasma Med.* **2013**, *1*, 24−29.

(5) Schlegel, J.; Köritzer, J.; Boxhammer, V. Plasma in Cancer Treatment. *Clin. Plasma Med.* **2013**, *1*, 2−7.

(6) Keidar, M. Plasma for Cancer Treatment. *Plasma Sources Sci. Technol.* **2015**, *24*, 33001.

(7) Metelmann, H.-R.; Nedrelow, D. S.; Seebauer, C.; Schuster, M.; von Woedtke, T.; Weltmann, K.-D.; Kindler, S.; Metelmann, P. H.; Finkelstein, S. E.; Von Hoff, D. D.; et al. Head and Neck Cancer Treatment and Physical Plasma. *Clin. Plasma Med.* **2015**, *3*, 17−23.

(8) Isbary, G.; Morfill, G.; Schmidt, H. U.; Georgi, M.; Ramrath, K.; Heinlin, J.; Karrer, S.; Landthaler, M.; Shimizu, T.; Steffes, B.; et al. A First Prospective Randomized Controlled Trial to Decrease Bacterial Load Using Cold Atmospheric Argon Plasma on Chronic Wounds in Patients. *Br. J. Dermatol.* **2010**, *163*, 78−82.

(9) Isbary, G.; Heinlin, J.; Shimizu, T.; Zimmermann, J. L.; Morfill, G.; Schmidt, H. U.; Monetti, R.; Steffes, B.; Bunk, W.; Li, Y.; Klaempfl, T.; et al. Successful and Safe Use of 2 min Cold Atmospheric Argon Plasma in Chronic Wounds: Results of a Randomized Controlled Trial. *Br. J. Dermatol.* **2012**, *167*, 404−410.

(10) Heinlin, J.; Isbary, G.; Stolz, W.; Morfill, G.; Landthaler, M.; Shimizu, T.; Steffes, B.; Nosenko, T.; Zimmermann, J. L.; Karrer, S. Plasma Applications in Medicine with a Special Focus on Dermatology. *J. Eur. Acad. Dermatology Venereol.* **2011**, *25*, 1−11.

(11) Dong, X.; Li, H.; Chen, M.; Wang, Y.; Yu, Q. Plasma Treatment of Dentin Surfaces for Improving Self-Etching Adhesive/Dentin Interface Bonding. *Clin. Plasma Med.* **2015**, *3*, 10−16.

(12) Kaushik, N. K.; Kim, Y. H.; Han, Y. G.; Choi, E. H. Effect of Jet Plasma on T98G Human Brain Cancer Cells. *Curr. Appl. Phys.* **2013**, *13*, 176−180.

(13) Vandamme, M.; Robert, E.; Lerondel, S.; Sarron, V.; Ries, D.; Dozias, S.; Sobilo, J.; Gosset, D.; Kieda, C.; Legrain, B.; et al. ROS Implication in a New Antitumor Strategy Based on Non-Thermal Plasma. *Int. J. Cancer* **2012**, *130*, 2185−94.

(14) Walk, R. M.; Snyder, J. A.; Srinivasan, P.; Kirsch, J.; Diaz, S. O.; Blanco, F. C.; Shashurin, A.; Keidar, M.; Sandler, A. D. Cold Atmospheric Plasma for the Ablative Treatment of Neuroblastoma. *J. Pediatr. Surg.* **2013**, *48*, 67−73.

(15) Gaur, N.; Szili, E. J.; Oh, J.-S.; Hong, S.-H.; Michelmore, A.; Graves, D. B.; Hatta, A.; Short, R. D. Combined Effect of Protein and Oxygen on Reactive Oxygen and Nitrogen Species in the Plasma Treatment of Tissue. *Appl. Phys. Lett.* **2015**, *107*, 103703.

(16) Hong, S.-H.; Szili, E. J.; Jenkins, A.; Short, R. D. Ionized Gas (Plasma) Delivery of Reactive Oxygen Species (ROS) into Artificial Cells. *J. Phys. D: Appl. Phys.* **2014**, *47*, 362001.

(17) Ishaq, M.; Kumar, S.; Varinli, H.; Han, Z. J.; Rider, A. E.; Evans, M. D. M.; Murphy, A. B.; Ostrikov, K. Atmospheric Gas Plasma-Induced ROS Production Activates TNF-ASK1 Pathway for the Induction of Melanoma Cancer Cell Apoptosis. *Mol. Biol. Cell* **2014**, *25*, 1523−31.

(18) Miller, M.; Lin, A.; Fridman, A. Why Target Immune Cells for Plasma Treatment of Cancer. *Plasma Chem. Plasma Process.* **2016**, *36*, 259−268.

(19) Khosravian, N.; Kamaraj, B.; Neyts, E. C.; Bogaerts, A. Structural Modification of P-Glycoprotein Induced by OH Radicals: Insights from Atomistic Simulations. *Sci. Rep.* **2016**, *6*, 19466.

(20) Dizdaroglu, M.; Jaruga, P. Mechanisms of Free Radical-Induced Damage to DNA. *Free Radical Res.* **2012**, *46*, 382−419.

(21) Takai, E.; Kitamura, T.; Kuwabara, J.; Ikawa, S.; Yoshizawa, S.; Shiraki, K.; Kawasaki, H.; Arakawa, R.; Kitano, K. Chemical Modification of Amino Acids by Atmospheric-Pressure Cold Plasma in Aqueous Solution. *J. Phys. D: Appl. Phys.* **2014**, *47*, 285403.

(22) Reisz, J.; Bansal, N.; Qian, J.; Zhao, W.; Furdui, C. M. Effects of Ionizing Radiation on Biological Molecules-Mechanisms of Damage and Emerging Methods of Detection. *Antioxid. Redox Signaling* **2014**, *21*, 260−92.

(23) Verlackt, C. C. W.; Neyts, E. C.; Jacob, T.; Fantauzzi, D.; Golkaram, M.; Shin, Y.-K.; van Duin, A. C. T.; Bogaerts, A. Atomic-Scale Insight into the Interactions Between Hydroxyl Radicals and DNA in Solution Using the ReaxFF Reactive Force Field. *New J. Phys.* **2015**, *17*, 103005.

(24) Van der Paal, J.; Verlackt, C. C. W.; Yusupov, M.; Neyts, E. C.; Bogaerts, A. Structural Modification of the Skin Barrier by OH Radicals: a Reactive Molecular Dynamics Study for Plasma Medicine. *J. Phys. D: Appl. Phys.* **2015**, *48*, 155202.

(25) Hawkins, C. L.; Davies, M. J. Generation and Propagation of Radical Reactions on Proteins. *Biochim. Biophys. Acta, Bioenerg.* **2001**, *1504*, 196−219.

(26) Xu, G.; Chance, M. R. Hydroxyl Radical-Mediated Modification of Proteins as Probes for Structural Proteomics. *Chem. Rev.* **2007**, *107*, 3514−3543.

(27) Yusupov, M.; Bogaerts, A.; Huygh, S.; Snoeckx, R.; van Duin, A. C. T.; Neyts, E. C. Plasma-Induced Destruction of Bacterial Cell Wall Components: A Reactive Molecular Dynamics Simulation. *J. Phys. Chem. C* **2013**, *117*, 5993−5998.

(28) Neta, P.; Huie, R.; Ross, A. Rate Constants for Reactions of Peroxyl Radicals in Fluid Solutions. *J. Phys. Chem. Ref. Data* **1990**, *19*, 413−513.

(29) Stadtman, E. R. Protein Oxidation and Aging. *Free Radical Res.* **2006**, *40*, 1250−1258.

(30) Lula, I.; Denadai, L.; Resende, J. M.; De Sousa, F. B.; Lula, I.; Santos, R. A. S. Study of Angiotensin-(1 − 7) Vasoactive Peptide and its B-cyclodextrin Inclusion Complexes: Complete Sequence-Specific NMR Assignments and Structural Studies. *Peptides* **2007**, *28*, 2199−2210.

(31) Bonechi, C.; Ristori, S.; Martini, G.; Martini, S.; Rossi, C. Study of Bradykinin Conformation in the Presence of Model Membrane by Nuclear Magnetic Resonance and Molecular Modelling. *Biochim. Biophys. Acta, Biomembr.* **2009**, *1788*, 708−716.

(32) Elstner, M.; Porezag, D.; Jungnickel, G.; Elsner, J.; Haugk, M.; Frauenheim, T.; Suhai, S.; Seifert, G. Self-Consistent-Charge Density-

DOI: 10.1021/acs.jpcc.6b12278
J. Phys. Chem. C 2017, 121, 5787−5799

Functional Tight-Binding Method for Simulations of Complex Materials Properties. *Phys. Rev. B: Condens. Matter Mater. Phys.* **1998**, *58*, 7260−7268.
(33) Gaus, M.; Cui, Q.; Elstner, M. DFTB3: Extension of the Self-Consistent-Charge Density-Functional Tight-Binding Method (SCC-DFTB). *J. Chem. Theory Comput.* **2011**, *7*, 931−948.
(34) Gaus, M.; Goez, A.; Elstner, M. Parametrization and Benchmark of DFTB3 for Organic Molecules. *J. Chem. Theory Comput.* **2013**, *9*, 338−354.
(35) de Vleeschouwer, F.; Geerlings, P.; de Proft, F. Radical Electrophilicities in Solvent. *Theor. Chem. Acc.* **2012**, *131*, 1−13.
(36) Abraham, M. J.; Murtola, T.; Schulz, R.; Smith, J. C.; Hess, B.; Lindahl, E. GROMACS: High Performance Molecular Simulations Through Multi-Level Parallelism from Laptops to Supercomputers. *Softw. X* **2015**, *1*, 19−25.
(37) Abraham, M. J.; van der Spoel, D.; Lindahl, E.; Hess, B.; and the GROMACS development team, GROMACS User Manual version 5.1.2, 2016.
(38) Golda, J.; Held, J.; Redeker, B.; Konkowski, M.; Beijer, P.; Sobota, A.; Kroesen, G.; Braithwaite, N.; Reuter, S.; Turner, M.; et al. Concepts and Characteristics of the 'COST Reference Microplasma Jet'. *J. Phys. D: Appl. Phys.* **2016**, *49*, 84003.
(39) Ellerweg, D.; von Keudell, A.; Benedikt, J. Unexpected O and O_3 Production in the Effluent of He/O_2 Microplasma Jets Emanating into Ambient Air. *Plasma Sources Sci. Technol.* **2012**, *21*, 34019.
(40) Hefny, M. M.; Pattyn, C.; Lukes, P.; Benedikt, J. Atmospheric Plasma Generates Oxygen Atoms as Oxidizing Species in Aqueous Solutions. *J. Phys. D: Appl. Phys.* **2016**, *49*, 404002.
(41) Yusupov, M.; Neyts, E. C.; Khalilov, U.; Snoeckx, R.; van Duin, A. C. T.; Bogaerts, A. Atomic-scale simulations of reactive oxygen plasma species interacting with bacterial cell walls. *New J. Phys.* **2012**, *14*, 093043.
(42) Lackmann, J.-W.; Baldus, S.; Steinborn, E.; Edengeiser, E.; Kogelheide, F.; Langklotz, S.; Schneider, S.; Leichert, L. I. O.; Benedikt, J.; Awakowicz, P.; et al. A Dielectric Barrier Discharge Terminally Inactivates RNase A by Oxidizing Sulfur-Containing Amino Acids and Breaking Structural Disulfide Bonds. *J. Phys. D: Appl. Phys.* **2015**, *48*, 494003.
(43) Espino, J. A.; Jones, L. M. In Cell Footprinting Coupled with Mass Spectrometry for the Structural Analysis of Proteins in Live Cells. *Anal. Chem.* **2015**, *87*, 7971−7978.
(44) Lins, L.; Thomas, A.; Brasseur, T. Analysis of Accessible Surface of Residues in Proteins. *Protein Sci.* **2003**, *12*, 1406−1417.
(45) Berlett, B. S. Protein Oxidation in Aging, Disease, and Oxidative Stress. *J. Biol. Chem.* **1997**, *272*, 20313−20316.
(46) Fletcher, G. L. Radiation-Induced Formation of Dihydroxyphenylalanine from Tyrosine and Tyrosine-Containing Peptides in Aqueous Solution. *Radiat. Res.* **1961**, *15*, 349−354.
(47) Maskos, Z.; Rush, J.; Koppenol, W. The Hydroxylation of Phenylalanine and Tyrosine: a Comparison with Salicylate and Tryptophan. *Arch. Biochem. Biophys.* **1992**, *2*, 521−529.
(48) Roeser, J.; Bischoff, R.; Bruins, A. P. Oxidative Protein Labeling in Mass-Spectrometry-Based Proteomics. *Anal. Bioanal. Chem.* **2010**, *397*, 3441−3455.
(49) Uchida, K. Histidine and Lysine as Targets of Oxidative Modification Review Article. *Amino Acids* **2003**, *25*, 249−257.
(50) Kato, Y.; Uchida, K.; Kawakishis, S. Oxidative Fragmentation of Collagen and Prolyl Peptide by Cu(II)/H2O2. *J. Biol. Chem.* **1992**, *267*, 23646−23651.
(51) Lermyte, F.; Martin, E. M.; Konijnenberg, A.; Lemière, F.; Sobott, F. *Analyzing Biomolecular Interactions by Mass Spectrometry*; Wiley-VCH Verlag GmbH & Co. KGaA: Berlin, 2015; pp 81−108.
(52) Konijnenberg, A.; Butterer, A.; Sobott, F. Native Ion Mobility-Mass Spectrometry and Related Methods in Structural Biology. *Biochim. Biophys. Acta, Proteins Proteomics* **2013**, *1834*, 1239−1256.
(53) Törnvall, U. Analytical Methods Methods. *Anal. Methods* **2010**, *2*, 1638.
(54) Kopito, R. R. Inclusion Bodies and Protein Aggregation. *Trends Cell Biol.* **2000**, *10*, 524−530.

NOTE ADDED AFTER ASAP PUBLICATION

This paper was published on March 10, 2017 with incorrect citations. The citations have been corrected and the paper was re-posted on March 16, 2017.

DOI: 10.1021/acs.jpcc.6b12278
J. Phys. Chem. C 2017, 121, 5787−5799